IOP Conf. Series: Materials Science and Engineering **604** (2019) 012069 doi:10.1088/1757-899X/604/1/012069

# Simulation studies of a coupled vane compressor

**K T Ooi [1,3] and P Shakya[2,4]**

[1, 2] School of Mechanical and Aerospace Engineering, Nanyang Technological University, 50 Nanyang Avenue, Singapore 639798

[3] mktooi@ntu.edu.sg
[4] pradeep005@e.ntu.edu.sg

**Abstract.** In this paper, the mathematical models of the novel Coupled Vane compressor (CVC) is formulated to study its operational characteristics and to assess its performance. Coupled Vane compressor, as the name implied, has two vanes coupled together. The unique feature of the compressor is that a set of two vanes are coupled together and they cut through the rotor diametrically. Theoretically, any rotor size which can accommodate the vanes will work with this design. This design removes most of the geometrical constraints imposed on the size of the rotor, as what happened in most of the rotary compressors. The ability to accommodate a significantly small rotor in this new design, makes it substantially more compact which also indirectly reduces material wastage, cost of machining and fabrication. This new design is intended to be used in refrigeration, household cooling and heating applications.

## 1. Introduction

Different types of the positive displacement compressor are used in air-conditioning, refrigeration, heating and air-compression applications. The rotary compressors, due to their simple construction, low noise and vibrations, are widely used in refrigerators and room air-conditioners. One of the common features exists in most of the rotary compressors available today is that they possess relatively large rotors as compared to the size of their cylinders, due to their design needs. The need for the large rotor has led to significant material wastage and large footprint. A new compressor design, namely, Coupled Vane Compressor (CVC) reduces the rotor size significantly, and hence the size of the cylinder, which resulted in a significantly more compact compressor. This new CVC is probably one of the most compact rotary compressors, if not the most compact one.

In a zero-dimensional modelling of a positive displacement compressor for performance prediction, the mathematical representations of the geometry of its working chamber, kinematics and dynamics of its mechanism, thermodynamics of its working fluid, main flows through inlet and discharge ports, secondary flows through internal leakages, lubrication of rubbing parts, heat transfer among the working fluid and the working chamber as well as among all other components may be considered.

In this paper, only the geometry and the thermodynamics model will be shown with considerable details. However, the overall results from the simulations will be presented and discussed.

## 2. Geometry model

The following sub-sections elaborate the formulations of the working chamber volume and the rate of change of volume of CVC at various vane angular positons. Each subsequent section takes care of

different region of the geometrical intricacies involved. Figure 1 illustrates the relevant cylinder and rotor volumes labelled $V_{c,st}$ and $V_{r,st}$ which are given by equations (1) and (2), respectively.

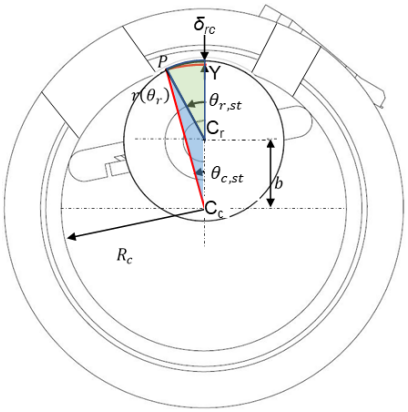


**Figure 1**. Illustration of the section of rotor and the cylinder to be deducted from the control volume

$$V_{r,st} = l_c\left(\pi R_r^2 \times \frac{\theta_{r,st}}{2\pi}\right) \tag{1}$$

$$V_{c,st} = l_c\left\{\left(\pi R_c^2 \times \frac{\theta_{c,st}}{2\pi}\right) - A_{C_R C_C P}\right\} \tag{2}$$

*2.1. Region where* $0° \leq \theta_r \leq \theta_{r,st}$

The $\theta_r = 0°$, is the position where the vanes coincide with the line joining the rotor centre $C_r$ and the cylinder centre $C_c$, and the chamber volume is zero, hence equations (3) and (4):

$$V(\theta_r) = 0, if\ 0 \leq \theta_r \leq \theta_{r,st} \tag{3}$$

$$\frac{dV(\theta_r)}{d\theta_r} = 0, if\ 0 \leq \theta_r \leq \theta_{r,st} \tag{4}$$

*2.2. Region where* $\theta_{r,st} < \theta_r \leq (180° + \theta_{r,st})$

The illustration of the suction chamber is shown in figure 2.

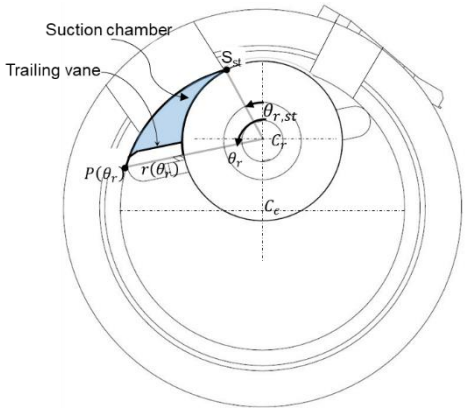


**Figure 2.** Illustration of the suction chamber at an arbitrary rotor angle

$$V(\theta_r) = \frac{l_c}{2}\left[R_c^2\theta_r + \frac{b^2}{2}sin(2\theta_r) - bsin\theta_r\{R_c^2 - (b\,sin\,\theta_r)^2\}^{\frac{1}{2}} - R_c^2\tan^{-1}\left(\frac{bsin\theta_r}{\{R_c^2 - (b\,sin\,\theta_r)^2\}^{\frac{1}{2}}}\right)\right]$$
$$-V_{c,st} - l_c\left\{\left(R_r^2 \times \frac{(\theta_r - \theta_{r,st})}{2}\right)\right\} - V_{t,vn}(\theta_r) \quad (5)$$

$$\frac{dV(\theta_r)}{d\theta_r} = \frac{l_c}{2}\left[R_c^2 + b^2cos(2\theta_r) - 2bcos\theta_r\{R_c^2 - (b\,sin\,\theta_r)^2\}^{\frac{1}{2}} - R_r^2\right] - \frac{dV_{t,vn}(\theta_r)}{d\theta_r} \quad (6)$$

*2.3. Region where (180° + $\theta_{r,st}$) < $\theta_r$ ≤ (360° - $\theta_{r,st}$)*

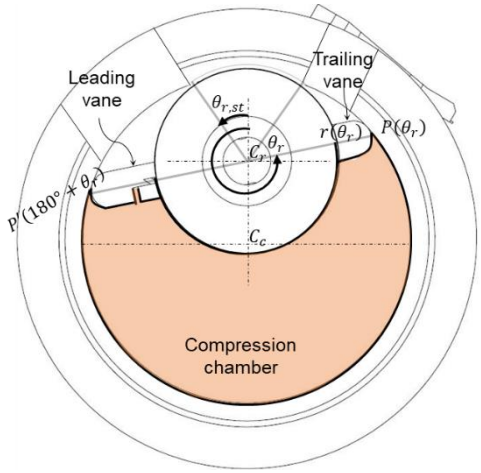


**Figure 3.** Illustration of the compression chamber at an arbitrary rotor angle

$$V(\theta_r) = \frac{l_c}{2}\left[R_c^2\pi - 2bsin\theta_r\{R_c^2 - (b\,sin\,\theta_r)^2\}^{\frac{1}{2}} - 2R_c^2\,tan^{-1}\left(\frac{bsin\theta_r}{\{R_c^2 - (b\,sin\,\theta_r)^2\}^{\frac{1}{2}}}\right)\right]$$
$$-l_c\left\{\frac{(\pi R_r^2)}{2}\right\} - V_{l,vn}(\theta_r) - V_{t,vn}(\theta_r) \quad (7)$$

$$\frac{dV(\theta_r)}{d\theta_r} = \frac{l_c}{2}\left[-4bcos\theta_r\{R_c^2 - (b\,sin\,\theta_r)^2\}^{\frac{1}{2}}\right] - \frac{dV_{l,vn}(\theta_r)}{d\theta_r} - \frac{dV_{t,vn}(\theta_r)}{d\theta_r} \quad (8)$$

*2.4. Region where (360° - $\theta_{r,st}$) < $\theta_r$ ≤(540° - $\theta_{r,st}$)*

$$V(\theta_r) = \frac{l_c}{2}\left[R_c^2(3\pi - \theta_r) + \frac{b^2}{2}sin(2\theta_r) + bsin\theta_r\{R_c^2 - (b\,sin\,\theta_r)^2\}^{\frac{1}{2}}\right]$$
$$+\frac{l_c}{2}\left[R_c^2\tan^{-1}\left(\frac{bsin(\theta_r - \pi)}{\{R_c^2 - (b\,sin\,\theta_r)^2\}^{\frac{1}{2}}}\right) - R_r^2(3\pi - \theta_r - \theta_{st})\right] - V_{c,st} - V_{l,vn}(\theta_r) \quad (9)$$

$$\frac{dV(\theta_r)}{d\theta_r} = \frac{l_c}{2}\left[-R_c^2 - b^2cos(2\theta_r) + 2bcos\theta_r\{R_c^2 - (b\,sin\,\theta_r)^2\}^{\frac{1}{2}} + R_r^2\right] - \frac{dV_{l,vn}(\theta_r)}{d\theta_r} \quad (10)$$

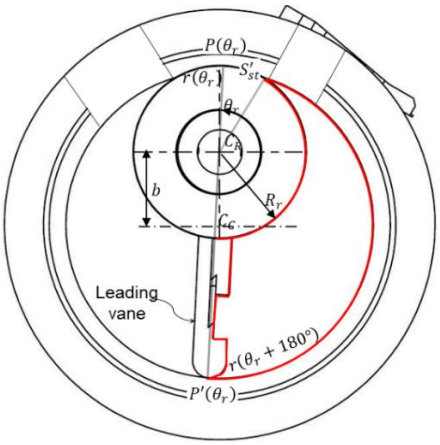


**Figure 4.** Illustration of the discharge chamber at an arbitrary rotor angle

*2.5. Region where* $(540° + \theta_{r,st}) < \theta_r \leq 540°$

In this region, no working volume is formed and hence equations (11) and (12):

$$V(\theta_r) = 0, if\ \left(540° - \theta_{r,st}\right) \leq \theta_r \leq 540° \tag{11}$$

$$\frac{dV(\theta_r)}{d\theta_r} = 0, if\ \left(540° - \theta_{r,st}\right) \leq \theta_r \leq 540° \tag{12}$$

As an illustration, take $b$ = 13 mm, $R_c$ = 27.5 mm, $R_r$ = 15.5 mm, $w_{vn}$ = 6 mm and $l_c$ = 30 mm, the variation of volume is shown in figure 5 (a). The maximum suction chamber volume is achieved at the rotor angle of 270°. In this case, this value is about 43.0 cm$^3$.

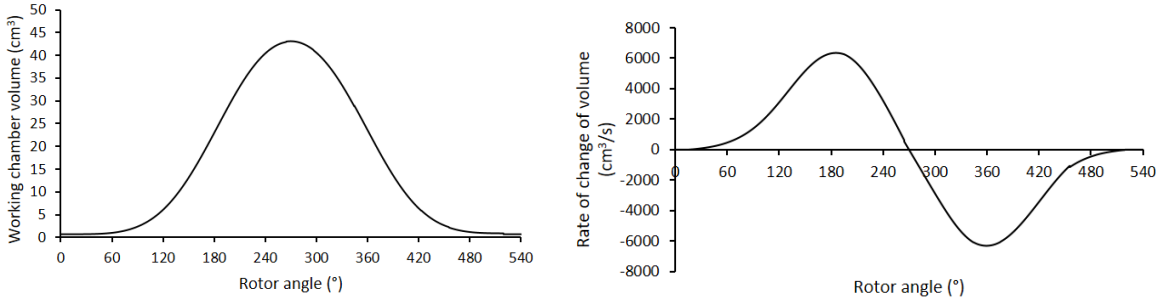


(a) Variation of chamber volume (b) Rate of change of chamber volume

**Figure 5.** Variation of the working chamber volume and the rate of change of the volume

The rate of change of volume with rotor angle is shown in figure 5 (b). From 0° to approximately 30° rotor angle, the volume remains constant, when it is within the sealing arc, an arc which was created to separate high pressure chamber from the low pressure chamber to reduce inter-chamber leakage. Apart from that a typical variations for volume and its rate of change are for a positive displacement compressor are depicted.

## 3. Special Vane Features

The operating principle of CVC has been described by Ooi and Shakya [1]. The illustrations of the vane geometries are shown in figures 6 (a) and (b). During the operation of the compressor, either of the

female or the male vane can assume the role of the leading or the trailing vane shown in figures 6 (c) and (d).

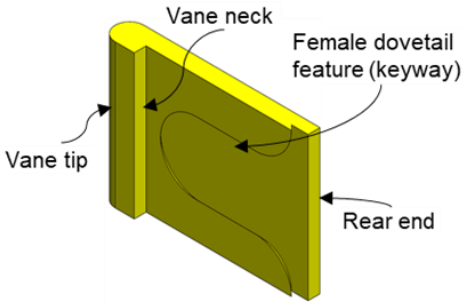


(a) A 3D view of a female vane

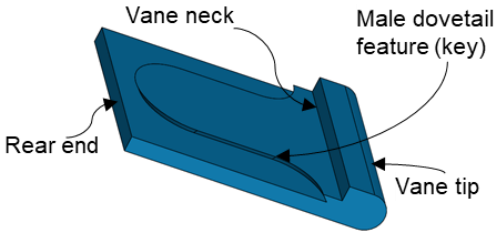


(b) A 3D view of a male vane

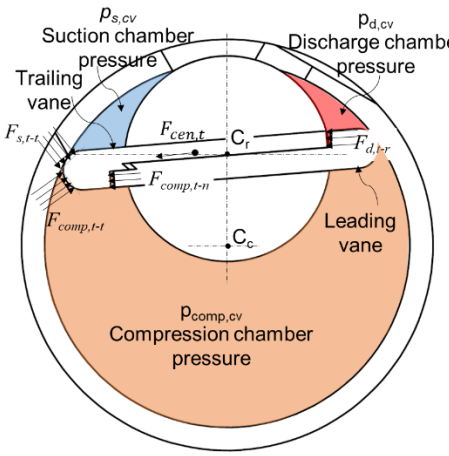


(c) Various forces acting on the trailing vane

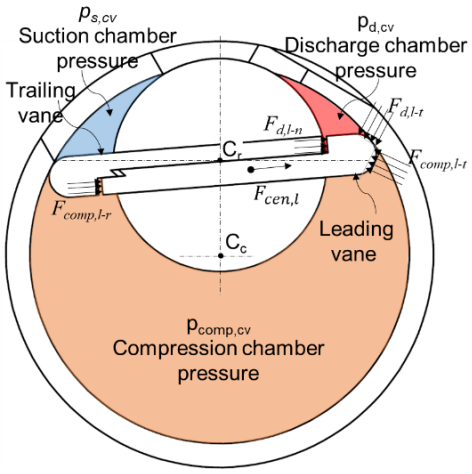


(d) Various forces acting on the leading vane

**Figure 6.** Illustrations of the vane designs and the various forces acting on the vanes during the operation

Both the vanes have three main parts, namely, vane tip, neck and the rear end. During the operation, the centrifugal forces on the vane ($F_{cen,t}$ and $F_{cen,l}$ in figures 6 (c) and (d) respectively) and the fluid pressure forces acting on the vane neck and the vane rear end ($F_{comp,t-n}$, $F_{d,t-r}$, $F_{d,l-n}$, $F_{comp,l-r}$ shown in figures 6 (c) and (d) respectively) press against the fluid pressure force acting on the vane tips $F_{s,t-t}$ and $F_{comp,t-t}$ on the trailing vane and $F_{d,l-t}$ and $F_{comp,l-t}$ on the leading vane. These vanes' specific geometry is designed to take advantage of centrifugal and fluid pressure forces, when exposed to high compression pressure, acting along the radial direction of the rotor, to strengthen the vane tips cylinder contact to prevent vane jump. This vane design, firstly, ensures the compression of the fluid without excessive leakage through the vane tips and secondly, allows the design flexibility to reduce the rotor diameter of CVC.

## 4. Thermodynamics model

In the formulation of the mathematical model, it is assumed that at any instant in time, the properties of the working fluid in the working chamber are uniform throughout spatially and any changes brought about by processes such as suction, compression and discharge are instantaneously propagated throughout the control volume. The flow processes involved are assumed quasi steady-flow. Employing

the First Law of Thermodynamic, the instantaneous changes of temperature and pressure of the working fluid in the working chamber are given in equations (13) and (14).

The suction and the discharge mass flowrates are modelled by assuming steady, isentropic, flow through an orifice [2].

$$\frac{dT_{cv}}{dt} = \frac{\left[\begin{array}{c} \frac{dq_{cv}}{dt} + \frac{dv_{cv}}{dt}\left\{V_{cv}\left(\frac{\partial p_{cv}}{\partial \rho}\right)_T - m_{cv}\left(\frac{\partial h}{\partial \rho}\right)_T\right\} + \frac{dm_{in}}{dt}\{h_{in} - h_{cv}\} \\ + \sum \frac{dm_{leak,in}}{dt}\{h_{leak,in} - h_{cv}\} \end{array}\right]}{m_{cv}\left(\frac{\partial h}{\partial T}\right)_\rho - V_{cv}\left(\frac{\partial p}{\partial T}\right)_\rho} \tag{13}$$

$$\frac{dp_{cv}}{dt} = \left(\frac{\partial p}{\partial T}\right)_\rho \frac{dT_{cv}}{dt} + \left(\frac{\partial p}{\partial \rho}\right)_T \frac{d\rho_{cv}}{dt} \tag{14}$$

The mass flowrate can then be written as shown in equation (15). An empirical coefficient, $C_d$, accounts for the actual non-isentropic flow and the flow loss. Additionally, the maximum flow velocity is considered occurred when the sonic velocity occurs at the throat of the flow port [3].

$$\dot{m} = \rho_{up} C_d A_{orifice}\left[2\left(h_{up} - h_{down,is}\right)\right]^{\frac{1}{2}} \tag{15}$$

## 5. Simulation results and discussions

For simplicity, assuming an adiabatic and perfectly sealed conditions, the variation of the fluid properties in the working chamber for an arbitrary size of a compressor are shown in figures 7 (a) – (e). The working fluid used was R1234yf. The fluid properties were evaluated using REFPROP subroutines [4]. The suction and the discharge temperature were set at 7.2°C and 54.4°C respectively. Figures 7 (a) – (c) show the variation of pressure, temperature and fluid mass in the working chamber during the suction, compression and discharge. The instantaneous variation of the power required to induce the fluid, compresses it and discharges it over one revolution of the rotor is shown in figure 7 (d). The peaks shown for two 'cycle' shown represents two chamber volumes per compressor cycle. For this arbitrary set of compressor dimensions, approximately 2.8 J of energy loss due to the over-compression during the discharge process. The total indicated work done to compress the gas was found to be 28.6 J.

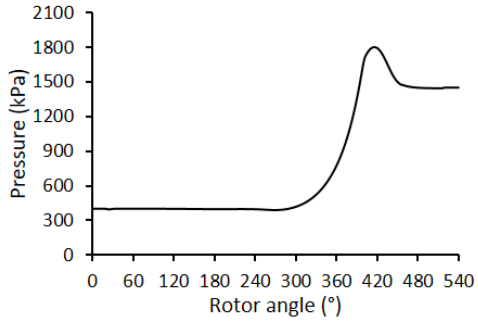


(a) Variation of working fluid pressure

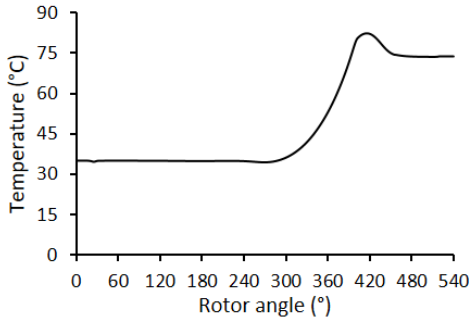


(b) Variation of working fluid temperature

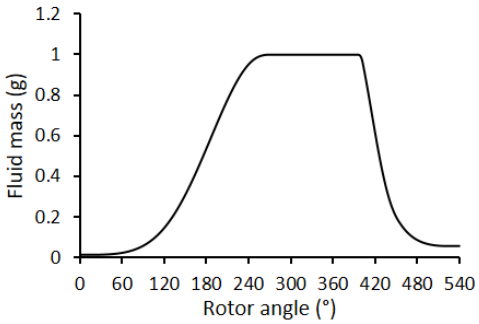


(c) Variation of fluid mass

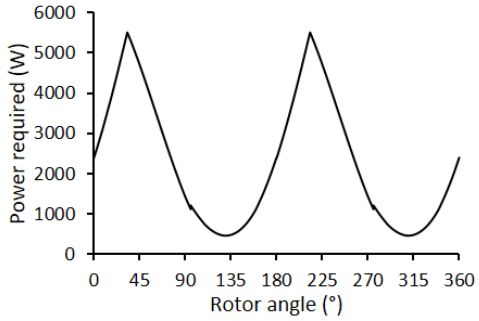


(d) Variation of instantaneous compression power

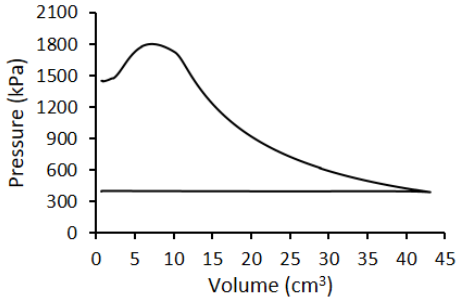


(e) Pressure-volume diagram

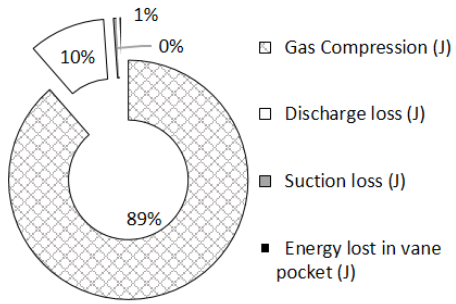


(f) Energy expended in gas compression

**Figure 7.** Variation of the properties from the numerical model

Figures 8 (a) and (b) show the variations of the predicted reaction force acting on the leading and the trailing vane tips as the resultant of the centrifugal force and the pressure forces acting on the various parts of the vane body. The friction coefficient of 0.1 (assuming dry contact between two polished steel) was assumed considering the frictional forces acting between the rotor slot and the vanes. The frictional forces act against the radial sliding of the vanes and act in the direction opposing the forces pressing the vane tips to the cylinder wall. In this study, it was also assumed that the fluid pressure acting at the sealing arc was equal to the average of the suction and the discharge pressure. In figure 8 (a), the predictions were calculated by varying the discharge to suction pressure ratio from 2 to 6 for the operating speed of 3000 r·min$^{-1}$. In figure 8 (b), the results were calculated by varying the operating speed of the compressor from 1000 r·min$^{-1}$ to 3000 r·min$^{-1}$ for the pressure ratio of 2. The results shown in figures 8 (a) and (b) are for 180° rotor angle because, the pressure forces are periodic every 180°. From figure 8 (a), it was found that the trailing vane and the leading vane tend to retract into the vane slot at the rotor angle positions from 0° to 17° and from 163° to 180° respectively. These positions occur when the vane tip departs from inner cylinder wall. From figure 8 (b), it was found that similar situation occurs at the same positions for the pressure ratio of 2 and the operating speed lower than 1000 r·min$^{-1}$. It was found that this situation occurs when the centrifugal forces acting on the vanes was found to have the least magnitude. However, the primary reason for the discontinuities at 17° and 163° rotor angle were mainly found to be due to the relatively low pressure was assumed at the sealing arc region, in this case, the average of the suction and the discharge pressure. The vane tips, when they were fully inside the rotor slot, were exposed to the pressure at the sealing arc. This meant that, the force acting on the vane tip became larger than the net pressure force acting on the vane neck and the vane rear end.

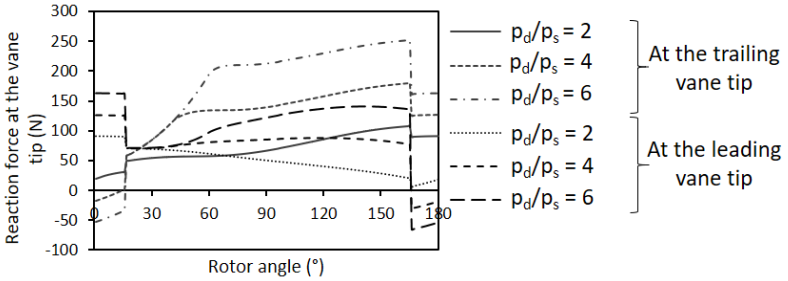


(a) Variation of the reaction forces at the vane tips for various discharge pressures

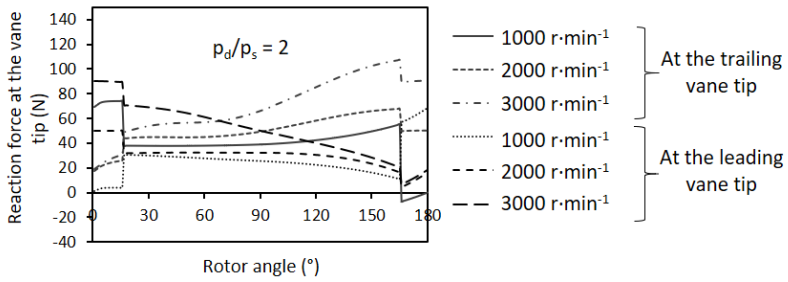


(b) Variation of the reaction forces at the vane tips for various operating speeds

**Figure 8.** Variation of the reaction forces for various operating conditions

## 6. Conclusion

The basic design, mathematical modelling and predictions of the geometry, vane dynamics and thermodynamics of the CVC using zero-dimensional model were presented. The special features of the vanes are also illustrated. The results obtained indicate the feasibility of CVC for the applications in air-conditioning, refrigeration, heating and air-compression. The unique feature of CVC is its coupled vanes which cut through the rotor and hence allowing the rotor radius to get significantly smaller as compared to all existing rotary compressors. Consequently, the cylinder and hence the overall size of the compressor reduces, thereby resulting in a compact compressor which saves significant amount of material and production cost. The prototype machine is currently in the fabrication. Once the measured results are available, further improvement in design is possible, which will lead to better compressor design. Using the available measured results, the prediction of compressor performance can be improved through a more comprehensive simulation model.

**Nomenclature**

| Alphabet | | Greek letters | |
|---|---|---|---|
| $b$ | Eccentric distance between the rotor center and the cylinder center (m) | $\delta$ | Depth of cut |
| $b$ | Eccentric distance between the rotor | $\theta$ | Angle (rad) |
| $h$ | center and the cylinder center (m) Specific enthalpy (J kg$^{-1}$) | $v$ | Specific volume (m$^3$ kg$^{-1}$) |
| $l$ | Length (m) | $\rho$ | Density (kg m$^{-3}$) |
| $m$ | Mass (kg) | $\omega$ | Angular velocity (rad s$^{-1}$) |
| $p$ | Pressure (Pa) | | |
| $q$ | Specific heat (J kg$^{-1}$) | Subscripts | |
| $r$ | Radial position with respect to the rotor center (m) | $c$ | Cylinder (-) |
| $w$ | Width (m) | $comp$ | Compression (-) |

| | |
|---|---|
| $A$ | Cross-sectional area ($m^2$) |
| $C$ | Centre (-) |
| $C_d$ | Coefficient of discharge (-) |
| $F$ | Force (N) |
| $R$ | Radius (m) |
| $T$ | Temperature (K) |
| $V$ | Volume (m) |

| | |
|---|---|
| *cv* | Control volume (-) |
| *d* | Discharge |
| *dov* | Dovetail feature |
| *down,is* | Downstream state assuming isentropic flow (-) |
| *in* | Flow in (-) |
| *l* | Leading vane (-) |
| *l-r* | Rear part of the leading vane |
| *l-t* | Tip of the leading vane |
| *leak,in* | Secondary flow (leakage) in (-) |
| *n* | Neck of the vane |
| *orifice* | Port orifice |
| *r* | Rotor (-) |
| rc | Rotor-cylinder interface |
| s | Suction |
| *st* | Start of the suction phase (-) |
| *t* | Trailing vane (-) |
| *t-r* | Rear part of the trailing vane |
| *t-t* | Tip of the trailing vane |
| *up* | Upstream (-) |
| *vn* | Vane (-) |

## References

1. Ooi K T and Shakya, P. (2018). A New Compact Rotary Compressor: Coupled Vane compressor. in *International Compressor Engineering Conference*. Paper 2613.
2. Jobson D A. (1955). On the Flow of a Compressible Fluid through Orifices. *Proceedings of the Institution of Mechanical Engineers*. **169**(1): p. 767-776.
3. Ooi K T, Chai, G B, and Kwek, E C. (1992). A simple valve model to study the performance of a small compressor. in *International Compressor Engineering Conference*. Paper 803.
4. Lemmon E W, Huber, M L, and McLinden, M O. (2010). NIST Standard Reference Database 23, Version 9.0. Thermophysical Properties Division (USA).